



Universiteit
Leiden
The Netherlands

Absorption, luminescence and scattering of single nano-objects

Yorulmaz, M.

Citation

Yorulmaz, M. (2013, June 26). *Absorption, luminescence and scattering of single nano-objects*. *Casimir PhD Series*. Retrieved from <https://hdl.handle.net/1887/21018>

Version: Not Applicable (or Unknown)

License: [Licence agreement concerning inclusion of doctoral thesis in the Institutional Repository of the University of Leiden](#)

Downloaded from: <https://hdl.handle.net/1887/21018>

Note: To cite this publication please use the final published version (if applicable).

Cover Page



Universiteit Leiden



The handle <http://hdl.handle.net/1887/21018> holds various files of this Leiden University dissertation

Author: Yorulmaz, Mustafa

Title: Absorption, luminescence, and scattering of single nano-objects

Issue Date: 2013-06-26

Influence of an approaching dielectric interface on the plasmon resonance of a gold nanorod

We study the effect of the distance between a gold nanorod and a glass surface on the plasmon resonance of a gold nanorod. To achieve this aim, we immobilize gold nanorods on one substrate, which is approached by the other one. These two substrates are bent rectangular cover-slides whose cylindrical axes are perpendicular to each other. We select a nanorod on the area where the two substrates can come into contact. In this geometry, a ring-shaped interference pattern (i.e. Newton's rings) appears at the contact area. The center of this pattern is determined prior to achieving contact between the substrates. Combining single-particle fluorescence spectroscopy and white-light interferometry, we follow the one-photon-excited luminescence spectrum of an individual nanorod as a function of the distance between the two substrates. We observe a significant red-shift of the surface plasmon for separation distances below 400 nm. This effect is reversible. Although the results are preliminary, this sensitivity of the plasmon resonance of a nanoparticle to its local dielectric environment may be useful in the study of interfaces between two solids and to map the contact areas between them.

6.1 Introduction

Studying the interactions between two approaching surfaces is essential for many scientific and technological applications. Materials with specific properties can be designed and developed to make miniaturized devices with optimal mechanical performance.^{106,220} For instance, wear in sliding contacts can be reduced using lubricants.^{221,222} Intermolecular and surface forces between moving or stationary bodies give rise to a resisting force against motion. In order to control friction between surfaces, it is necessary to investigate the structure of the contact area.^{105–107} All surfaces in nature have roughness, which extends over many different length scales, from atomic (\sim nm) to macroscopic dimensions (\sim mm). These complex heterogeneities of the contacting interfaces make the interactions between the two bodies difficult to study.

Early experiments to understand these complex interactions have been started as early as 1699 by Amontons. He used different materials (i.e. iron, lead, wood) in different combinations and measured the force necessary to bring a plate to slide on another plate. He found the friction force to be directly proportional to the applied load and independent of the macroscopic contact area.²²³ By 1781, the distinction between static and kinetic friction was made by Coulomb. He studied the friction between sliding surfaces of different materials and considered the effect of sliding velocities on the friction. Coulomb is often credited with the third law of friction, which states that the kinetic friction force is nearly independent of the sliding velocity. Later, Hertz's theory suggested that the contact area would increase nonlinearly with the applied load under elastic deformation.²²⁴ After the pioneering work of Hertz,²²⁴ the experimental and theoretical effort was increased to study the real contact area between two solids that are brought together. For example, surfaces of elastic materials were reported to present many irregularities.^{109,225} Bowden and Tabor suggested the presence of a number of small spherical contact points (asperities) which are uniformly distributed within the boundary of macroscopic contact.¹⁰⁹ The sum of the contact areas at asperities was then suggested to be smaller than the apparent contact area. This assumption was refined by Archard who showed that small asperities could also be present on each asperity.²²⁵ According to this latter model, the increasing number of contacting asperities at the interface results in a near

proportionality of the contact area to the load. A more detailed model than the previous one was presented by Greenwood and Williamson¹¹⁰, who took into account a Gaussian distribution of asperity heights and possible deformation of high asperities.²²⁴ They also predicted the real contact area to be nearly proportional to the applied load. Because surfaces exhibit roughness on different length scales, the real area of contact is different from the apparent contact area.^{107,110,112,226-228}

In recent studies, the tribological interactions that take place at solid-solid or solid-liquid-solid interfaces have been studied by sensitive scanning probe and optical microscopy techniques.²²⁹⁻²³⁶ In scanning probe techniques, topography images are usually obtained by recording the distance-dependent changes of probe-sample interactions. The standard approach to study the real contact area between solids at molecular scales has been conventional atomic force microscopy (AFM)²³⁷. This technique can provide topography images of a solid surface with a very high resolution, down to atomic scale.²³⁸ However, the contact in AFM studies takes place between the AFM tip and the very local region under the tip.²³⁹ The deformation under and around the tip may be very different from the deformation of the bodies in the extended contact areas. Moreover, the information obtained from AFM topography images depends very much on the tip shape and on the path the tip follows.^{113,239-241}

Optical microscopy measurements are usually noninvasive and can provide a larger field of view than scanning probe microscopy.^{112,231,242} The surface force apparatus of Israelachvili²³¹ is used to measure the forces between two solid surfaces usually immersed in a liquid (e.g. Van der Waals and electrostatic forces). This instrument consists of two curved surfaces and sensitive force-measuring leaf springs. In this method, the forces between curved surfaces are measured while one of the two surfaces is approached or retracted. The forces measured can be as weak as 10^{-8} N. The distances between the two surfaces are measured using optical interferometry, down to 0.3 nm.²⁴³ For a reliable measurement, atomically smooth surfaces (i.e. mica) are needed. Uses of the surface force apparatus are therefore restricted to special measurement conditions and samples.

In a recent study of Krick. et. al¹¹², interferometric optical measurements and mechanical measurements were combined by an optical in-situ tribometer. They used changes in the intensity of 0th order Newton's rings to probe

the complex area of contact between a rubber sphere and a polished glass flat. The intensity reflected by the interface between two solids (at least one of them has to be transparent) monotonically decreases for air gaps less than a quarter of a wavelength. Monitoring this reflection in a wide-field image, Persson and coworkers¹¹² could map the separation between two surfaces. However, in wide-field imaging, removing reflection contributions from other, off-focus interfaces is difficult. Therefore, they had to subtract a background image (obtained when sphere and glass were not in contact) from the contact image (when sphere and glass were in contact). In this way, they obtained topography images for different applied loads (mN), but, because of the noise in the subtraction, they could not measure very small gaps accurately. They applied this method mostly to determine the roughness of the rubber sphere, which was on the order of a few μm . For quantitative determinations of very small gaps, it would be advantageous to use confocal scanning instead of wide-field imaging.

Another example of optical imaging of topography is the well-known technique of frustrated total internal reflection microscopy.^{242,244} In this technique, evanescent waves are created at a plane interface by total internal reflection of light of wavelength λ , and a second parallel plane interface is approached towards the first one. For distances below the typical decay length of the evanescent wave between the two interfaces, evanescent waves interact with the second interface and can be partly transmitted as propagating radiation. The relative intensity of the transmitted light depends on the distance between the two substrates. The transmitted intensity exponentially decreases for increasing gap widths.²⁴⁴ Therefore, transmission measurements will provide accurate measurements of large gaps (provided the transmitted intensity is still measurable). Conversely, reflection vanishes for vanishing gaps and will be very sensitive to small gaps (see previous discussion). Shallow topographic features with sizes smaller than $\lambda/2\pi$ or smaller were detected using this method.²⁴² Small gaps can also be measured in a similar way by observing the reflection at normal incidence.

Sensitive plasmonic sensors^{14,119,245} can be applied for measuring distances between two substrates, and might be useful to improve the lateral resolution of measurements of the contact area. These sensors exhibit a very high sensitivity to refractive index changes,⁷⁸ because their plasmon resonance is highly sensitive to the dielectric environment.^{25,31,246} The sensitivity

of gold nanorods to local environmental changes has been exploited in numerous applications.^{14,25,119,247,248} In these studies, nanorods served as transducers of molecular binding events in biological or chemical experiments. Their signals are also sensitive to the changes in their orientation.¹⁴⁹ Moreover, gold nanorods are easy to synthesize and they can cover larger areas than those probed by scanning probe measurements. For this purpose, it is important to study the sensitivity of single gold nanorods to nearby surfaces.

In our study, we investigate the response of the gold nanorod with respect to an approaching glass substrate. We use two curved glass substrates whose longitudinal axes are oriented perpendicular to each other (so called "crossed-cylinder" geometry²³¹). We immobilize gold nanorods on one glass substrate and deposit a thin layer of PMMA on the other substrate. We perform luminescence spectroscopy on a single gold nanorod to study the distance dependence of its plasmon resonance. Changes in the refractive index of the medium affect the optical properties of the gold nanorods,²⁴⁹ i.e., the plasmon resonance wavelength red-shifts for decreasing gaps between the glass substrates.^{14,250} The observed changes are related to the rapid decay of the electromagnetic near fields away from the surface of the gold nanorod^{14,251} and to the interactions of plasmon with the mirror image of the nanorod in the nearby dielectric surface.²⁵⁰ We show that the gold nanorod exhibits distinct changes in its plasmon resonances. Gold nanorods can find applications for sensing in biology or tribology studies as they exhibit distinct changes in their plasmon resonances by the variations in the local nm-scale environment.

6.2 Methods and materials

6.2.1 Fluorescence spectroscopy and white-light interferences

We performed fluorescence spectroscopy measurements on our home-built variable-distance cell, assembled on an inverted microscope. The schematic of the setup is shown in Fig.6.1. Circularly polarized light (476 nm) is used for fluorescence excitation. The beam is expanded to ~ 20 mm and reflected off from a 20R/80T beam-splitter towards an oil-immersion microscope objective (Olympus, 60 \times , 1.45 NA). The excitation light is focused by the objective to a diffraction-limited spot (about 300 nm in diameter) for excitation

6 Influence of an approaching dielectric interface on the plasmon resonance of a gold nanorod

of individual gold nanorods. The luminescence from nanorods and backscattered excitation light are collected by the same microscope objective and they are transmitted through the beam splitter. The luminescence is filtered out from the excitation light by long-pass filters (LP02-514RS-25, Semrock and NF476, AHF) and is spatially filtered by a $75\ \mu\text{m}$ pinhole. Luminescence images and spectra of the same individual nanorods are respectively detected by an avalanche photodiode and by a spectrometer with the help of a mirror installed on a flip mount. During luminescence measurements, nanorods are immobilized on one glass substrate, which can be approached by another one (see Section 6.2.2).

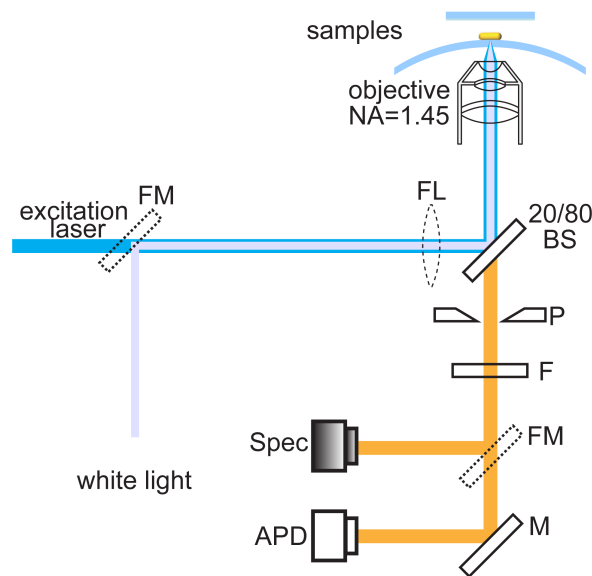


Figure 6.1: Schematic of the experimental setup. FM-flip-mirror; FL-flip-lens; NA-numerical aperture; BS-beam-splitter; P-pinhole; F-filter; M-mirror; APD-Avalanche photodetector; Spec-Spectrometer.

For recording white-light interference, a 100 W halogen lamp is used as the light source. The white light is focused at the back focal plane of the microscope objective (Olympus $60\times$, 1.45 NA or Olympus $10\times$, 0.4 NA). This way, a collimated beam in the air gap within the two substrates is obtained. An interference pattern (fringes) is created by the interference of reflected waves from the air-glass interfaces. The interference spectra are recorded using a spectrometer and used for measuring air-gap widths between the sub-

strates (see Section 6.3.1, Figure 6.5). White-light interference images are also recorded. The obtained image represents the well-known Newton's rings, which are useful to find the contact area (see Section 6.3.1, Figure 6.4).

6.2.2 Variable-distance cell

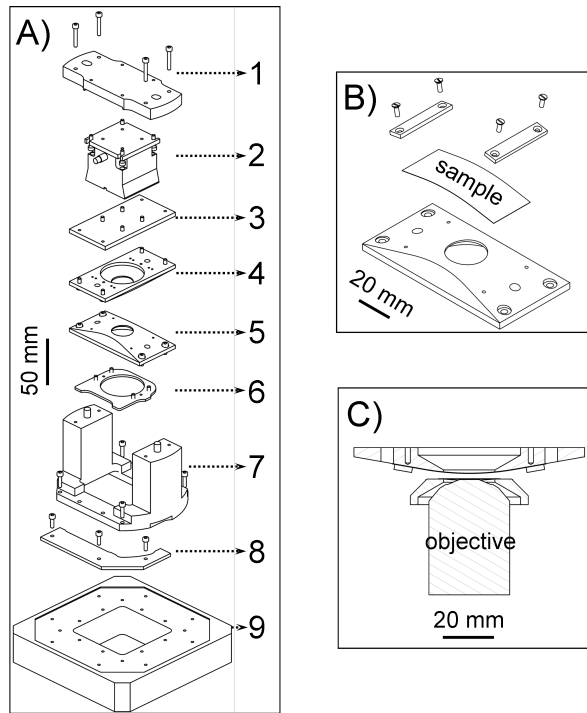
We used a variable-distance cell to change the distance between the two substrates so that we could study the influence of nanorod-substrate distance on the plasmon resonance of a gold nanorod. The variable-distance cell is formed of two curved sample holders, two three-axis (xyz) piezo-stages and several aluminum adapters. We use two rectangular BK-7 glass slides ($25\text{mm} \times 60\text{mm} \times 160\mu\text{m}$) that are installed on curved aluminum sample holders of radius of curvature $R \approx 100\text{ mm}$ (Fig.6.2 B). The curved rectangular substrates are positioned such that their long axes are perpendicular to each other and they can approach each other (Fig.6.2 C). This geometry is called "crossed-cylinders configuration" and frequently used in wear (friction) experiments.²³¹ The crossed-cylinders configuration is advantageous because its geometry is equivalent to that of a flat surface and a sphere of radius R . The apparent contact area can be calculated taking into account the applied load and the radius of curvature of the substrates. Moreover, alignment with crossed-cylinder geometry is much easier than with two flat substrates, i.e., two curved substrates come in contact at the place of 0th order Newton's rings (see Section 6.3.1, Fig.6.4).

In order to set up the variable-distance-cell, the curved sample holder with one substrate (bottom sample) is initially attached to a PI-MARS piezo-stage (Fig.6.2 A, component 9). The sample holder is made so that bottom sample can be approached by an objective from beneath for optical spectroscopy (Fig.6.2 C).

The other substrate (top sample) on the other curved sample holder is installed on a different piezo-stage (PI-NanoCube), which is attached to a rectangular aluminum adapter plate. This configuration is supported by two (attached) aluminum blocks such that the top sample faces the bottom sample. We call this design bridge configuration (Fig.6.2 A, components 1-4,7).

During the installation process, the bottom sample and the bridge configuration (which includes the top sample) are consecutively installed on the same piezo-stage (PI-MARS) such that the two substrates can be moved si-

Figure 6.2: A) Components of the variable-distance-cell 1) Aluminum adapter plate to which PI-NanoCube is mounted. 2) PI-NanoCube piezo-stage. 3) Adapter plate for sample mount. 4) Top sample holder. 5) Bottom sample holder. 6) Kinematic platform for bottom sample holder. 7) (Attached) aluminum blocks. 8) Kinematic platform for bridge configuration (1-4,7). 9) PI-MARS piezo-stage. B) Sample holder and cover glass with mounting adapters C) Side view of two sample holders with microscope objective.



multaneously. The design also allows moving the top sample separately with respect to the bottom sample along three axes while keeping the position of the bottom sample the same. Moreover, two kinematic platforms (Fig.6.2 A, components 6, 8) help for precise positioning of the two samples if samples need to be installed and re-installed with high repeatability. They are convenient whenever the sample has to be removed, for example to change the objective.

After the installation of the two samples, it is necessary to find the contact area to start spectroscopy measurements. This procedure may require lateral movement of both samples for distances ranging from several $100 \mu\text{m}$ to a few millimeters. Therefore, the variable-distance cell is attached to a manual xy translation stage, which is used for coarse lateral movements of both samples with respect to the microscope objective.

During the optical study of gold nanorods, we keep the variable-distance cell in a thermocol box with thick walls ($\sim 30 \text{ mm}$). We use the box to minimize possible small thermal drift (a few 100 nm/K) of piezo-stages. The box partly isolates the variable-distance cell from the room, thereby minimizing

temperature variations during the optical measurements.

6.2.3 Samples

We spin-coated single gold nanorods on one glass substrate for optical microscopy measurements and we used this substrate with nanorods as the bottom sample. The gold nanorods used in this study were prepared in a seed-mediated growth method.²¹⁴ The ensemble average aspect ratio of the nanorods is about 2.2. The ensemble average width and length of the nanorods are 30 nm and 65 nm, respectively. The absorption spectrum of the nanorods suspension is shown in Fig. 6.3. An SEM image of the nanorods is shown in the inset of Fig. 6.3.

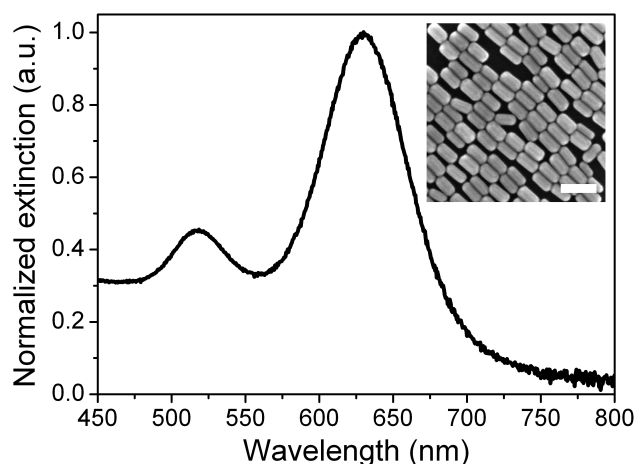


Figure 6.3: Extinction spectrum of gold nanorod suspension in water. There are two peaks. The red-most plasmon resonance corresponds to the longitudinal plasmon resonance of gold nanorods. The blue-most peak is formed by contributions from both transverse plasmon resonance of gold nanorods and residual gold nanospheres in the suspension. The inset shows an SEM image of the sample used in this study. The ensemble average width and length of the nanorods are 30 nm and 65 nm. The scale bar in the inset SEM image is 100 nm.

The top sample is prepared by spin-coating 15 mg/mL PMMA/toluene solution at 4000 rpm for 90 s. This procedure yields a (~ 25 nm) thick PMMA layer on glass, which helps to suppress stiction between the glass substrates.

Surfaces, which come in close proximity, may adhere to each other. This stiction, or static friction, arises from various forces between the two surfaces, including Van der Waals forces, electrostatic forces, and capillary forces from a liquid (water) bridge.²³² Stiction complicates the distance-dependent measurements because extra force (stiction force) is required to overcome the adhesion to enable relative motion of two surfaces. Moreover, if the two substrates are in close proximity of each other, they may uncontrollably come into contact. Capillary forces are often the dominant adhesive forces, and they are usually responsible for the stiction. They give rise, e.g. by condensation of water vapor, to a liquid bridge between the two solids. In this case, stiction may be reduced by minimizing the surface energy, the amount of liquid present at the interfaces and/or the contact area between the surfaces.²⁵² Surface energy can be reduced by using a hydrophobic surface²⁵² and the thin hydrophobic PMMA layer on the top sample was found to reduce the stiction during spectroscopy measurements.

We were also careful to minimize the dust deposition on the prepared samples. After we prepared the samples, we put them directly in a sealed box and transferred them to the laboratory. We then quickly installed them on sample holders which we installed in the variable-distance cell to conduct optical spectroscopy of single gold nanorods.

6.3 Results and discussions

6.3.1 Newton's rings and distance measurement

After samples were prepared, we installed them in the variable-distance-cell as described in Section 6.2.2. We performed single-particle spectroscopy after we found the local minimum of the distances between the two substrates. We first recorded interferences of the white light on a CCD, which showed the well-known Newton's rings (Fig. 6.4). We used a different objective (Olympus 10X, 0.4NA) because the size of the Newton's rings formed in this geometry was larger than the image sizes obtained by 60 \times magnification objective.

We observed Newton's rings when the distance between the two substrates was less than half of the coherence length of the white light (about 2 micrometers). Newton's rings consist of colored concentric rings. This is because different wavelengths of each color constructively interfere (in re-

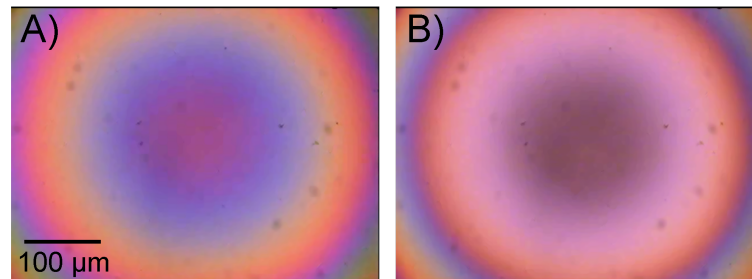


Figure 6.4: Newton's rings formed when the two substrates are in A) optical contact; B) mechanical contact. The contact area should be completely black, but a background from out-of-focus reflections remains.

flection) at different air-gap thicknesses, which increases outward from the center of the rings (Fig. 6.4 A). We used the Newton's rings to find the local-minimum distance, as the center of the Newton's rings is the point where the distance between the two crossed-curved substrates is minimum.

We first have to find the Newton's rings and overlap their center with the center of the microscope objective's field-of-view. This procedure ensures that the optical measurements will be done at (or close to) the point where the two surfaces will first get into contact. This is important in order to relate the piezo-stage translation to the gap size in a simple way. Indeed, if the same measurement is done at a point away from the point of first contact, it may not be possible to achieve contact. Moreover, because the two substrates already get into contact elsewhere, they will deform in complicated ways upon further approach, making the relation between piezo-stage displacement and gap nonlinear and uncontrollable.

At the optical contact, the two substrates do not physically touch each other. Alternating colors of Newton's rings are observed for varying distances below about $2 \mu\text{m}$. When the distance between the two substrates is further decreased, a transition from optical contact to mechanical contact is observed (Fig. 6.4A-B). At the mechanical contact, the center area of Newton's rings turns black due to destructive interference of the white-light since the path difference is zero (Fig. 6.4 B). This dark spot is used to detect mechanical contact and check the circular shape of the contact area.¹¹² The size of the dark spot increases with the radius of curvature of the two glass substrates and with the load applied to the substrates.¹¹²

The distance between the two surfaces can be determined by record-

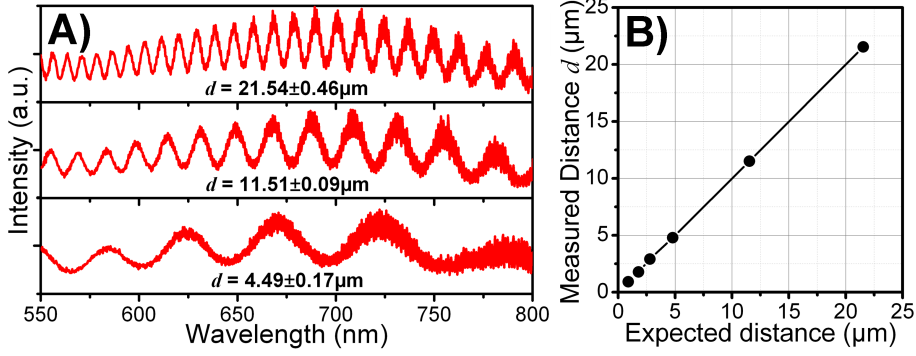


Figure 6.5: (A) Fringes of the reflected white light from the friction cell at different air-gap thickness. Distances (B) Characterization of the piezo stage movement and the distance measurement.

ing the spectrum of the reflected light (interference fringes) as shown in Fig. 6.5 A. The distance (d) is estimated from the fringe spectrum by averaging all distances obtained from each pair of consecutive peak wavelengths (λ_1 and λ_2) according to Eq. 6.1 using Matlab. For different separation distances of two substrates, the calculated distances with standard deviations of the mean are depicted in Fig. 6.5 A.

$$d = \frac{\lambda_1 \lambda_2}{2|\lambda_1 - \lambda_2|} \quad (6.1)$$

In order to check for the linearity of the PI-NanoCube movement, we measured the distance as described above while we were moving the top sample. We plotted the measured distance as a function of the expected distance Fig. 6.5 B. We measured the distance for six piezo-steps as shown in Fig. 6.5 B, which shows a linear movement. We relied on piezo-movement for distances below $1 \mu\text{m}$ since distances below $1 \mu\text{m}$ could not be measured by white light interferences.

We also recorded the fringes continuously while we were simultaneously moving the two samples in lateral directions using the manual xy translation stage. We followed the number of fringes in the interference spectrum so that we could find a point very close to the minimum-distance point. In order to get rid of any uncontrolled mechanical contact of the nanorod with the top substrate during the course of these lateral motions, we kept several tens of micrometers spacing between the two substrates.

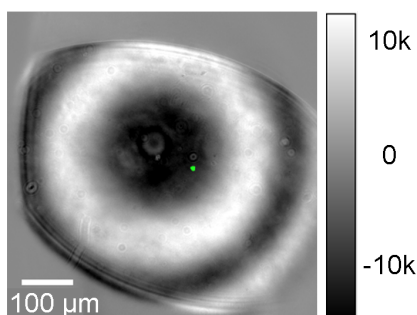


Figure 6.6: Overlap of the small green laser spot and the Newton's rings

After finding the first-contact area, we focused the laser on the same area of the bottom sample and looked for a nanorod to record its spectrum. After finishing the single-nanoparticle spectroscopy measurements, we checked the overlap again by imaging the Newton's rings (Fig.6.6). The measurement point is shown as a small green dot in Fig.6.6. In our experiments, the distance between the laser spot and the center of the Newton's ring was about $75 \mu\text{m}$. We calculated that the distance between the two substrates at the imaging point was 30 nm when the two substrates first got in mechanical contact at the minimum-distance point. For distances lower than 30 nm , we can no longer ensure the linearity of the gap as a function of the piezo-stage movement (Fig. 6.5 B).

6.3.2 Plasmon resonance as a distance ruler

In order to characterize the response of the gold nanorod to an approaching dielectric interface, we studied its luminescence spectrum. We initially recorded the luminescence spectrum of the gold nanorod when the distance between the substrates was about $30 \mu\text{m}$. This spectrum served as reference for infinite gap width. We had to check whether the mechanical contact led to any irreversible change of the nanorod spectrum. Therefore, we checked for changes of the spectrum and of the orientation of the nanorod after mechanical contact with the top substrate. Thus, we recorded the spectra of the nanorod at different detection polarizations before and after the substrate was in contact with the top substrate (see Fig. 6.9 B). We measured the polarization anisotropy and determined the orientation of the nanorod for both cases.

A luminescence spectrum and an image of a nanorod at about $30 \mu\text{m}$ separation of the substrates is shown in Fig. 6.7. The color scale of the luminescence image shows the luminescence count-rate of the nanorod, which was excited at 476 nm at an intensity of $360 \text{ kW}/\text{cm}^2$. We obtained the full-width-at-half-maximum of the luminescence spot along the x - and y -axis by a Gaussian fit. This yielded values for σ_x and σ_y of 390 nm and 340 nm for the luminescence spot, respectively. We also recorded the luminescence spectrum of the gold nanorod (Fig. 6.7). We checked that we had a single gold nanorod by looking at its spectral shape, a single Lorentzian profile (see Chapter 5).

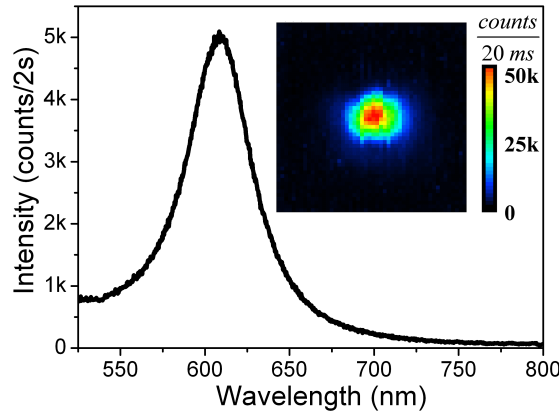


Figure 6.7: Luminescence spectrum of a single gold nanorod. The spectrum was recorded in air on glass substrate with 476 nm excitation at $360 \text{ kW}/\text{cm}^2$ in 2 s. The plasmon resonance of the nanorod is 608.8 nm . The inset shows the luminescence image of the nanorod, which was excited under the same conditions as of the spectrum. The size of the image is $2 \mu\text{m}^2 \times 2 \mu\text{m}^2$ ($20\text{ms}/\text{pixel}$, 40 nm pixel size).

We started to successively record the spectrum of the single gold nanorod when the spacing between the two substrates was $1.4 \mu\text{m}$. We moved the top piezo-stage step by step, thereby moving the top sample towards the stationary bottom sample. The step size of the movement was 50 nm . Because the piezo-stage moves linearly (See Fig.6.5 B), we assume that the distance between the two substrates was decreased by 50 nm at each step. It is important to keep in mind that the linear movement could only be achieved for spacings larger than 30 nm (see Section 6.3.1, Fig. 6.6). We show the results of our experiment in Fig. 6.8 where we plot the luminescence spectra of the

same nanorod for different air-gap sizes. The arrow in the figure indicates the direction of the decreasing distance.

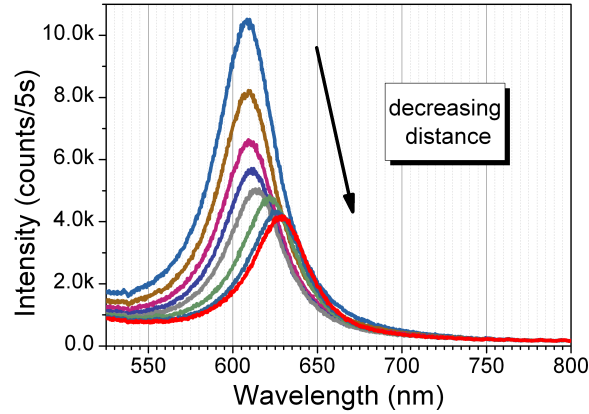


Figure 6.8: The change in the luminescence spectrum of the nanorod when the nanorod is approached with a second glass substrate from the top.

Fig. 6.8 clearly shows red-shifted plasmon resonances for decreasing distances. The observed red-shifts can be attributed to an increase in the effective refractive index.^{71,73} While two substrates are getting closer, polarization charges in the approaching dielectric shield the surface plasmon field and reduce the oscillation frequency of the longitudinal plasmon. We also observe a decrease in the detected photoluminescence intensity of the nanorod for decreasing separations of the two substrates. It can be attributed to the change in the radiation pattern of the nanorod due to the approach of the second dielectric interface.²⁴⁴ The radiation pattern of the dipole in an air gap between two planar interfaces depends on the dipole's orientation, the dipole's position within the gap, and the refractive index of the dielectric.²⁴⁴ For large separation distances between the substrates, we can assume that the nanorod is immobilized at the air-glass interface (refractive indices $n_{glass} \approx 1.5$ and $n_{air} \approx 1$). Under this condition, most of the luminescence intensity of the nanorod is radiated towards the high-refractive-index side. When the upper interface touches the gold nanorod, the nanorod's radiation pattern becomes symmetrical and equal amounts are emitted in both glass slides.²⁵³ The amount of light emitted in the bottom slide and detected will therefore decrease during the approach.

6 Influence of an approaching dielectric interface on the plasmon resonance of a gold nanorod

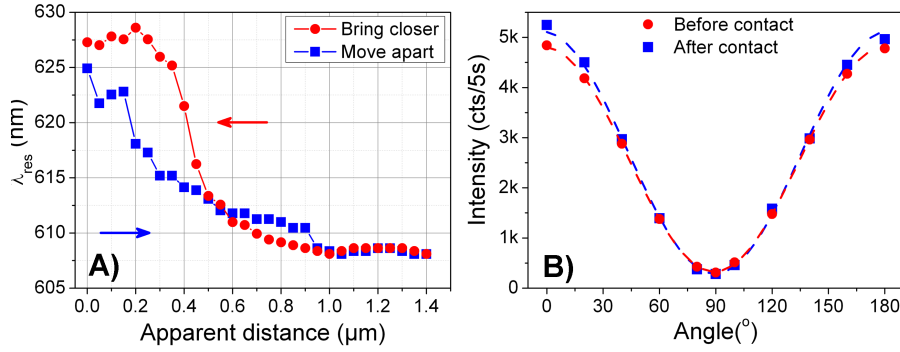


Figure 6.9: (A) The plasmon resonance wavelength λ_{res} as a function of the apparent distance between the two substrates. (B) Longitudinal plasmon resonance intensity as a function of the analyzer angle. For both images red-circles represent data which are obtained while decreasing the distance between the two substrates. The blue-square data is of experiment when the top substrate was retracted.

In Fig.6.9 A, we plot the plasmon resonance (λ_{res}) as a function of the apparent distance between the two substrates. For distances smaller than 1 μm , we estimated the apparent distance from the movement of the piezo-stage. The upper substrate was moved first towards the lower substrate until contact, then back, and spectra were recorded during the two movements to check the reversibility of the plasmon resonance wavelength change. The red points in Fig.6.9 A refer to the approach of the upper substrate, whereas the blue points were measured upon retraction. We note that the shift curve upon retraction differs from the shift curve upon approach. This may arise from hysteresis of the piezo stage, or from irreversible modifications of the substrates upon contact. For example, a capillary bridge can form, or plastic deformation of the PMMA layer can take place. For this reason, we consider only the first approach curve (red points in Fig.6.9 A). This approach curve shows a distinct shift for distances less than 1 micron, which regularly increases until the distance of 350 nm. At smaller distances, the shift remains essentially constant. The weak changes of the shift which are still observed below 350 nm may be due to interaction of the nanorod with the approaching PMMA layer, in a similar way as was observed by Novo et al.¹²¹ We attribute the change of behavior of the shift at ~ 350 nm to the first contact between the two substrates. We therefore deduce the actual distance between the substrates according to $s = [\text{Apparent distance}] - 350$ nm, and can plot the mea-

sured shift $\Delta\lambda = \lambda_{measured} - \lambda_0$ as a function of this distance s , as shown in Fig.6.10.

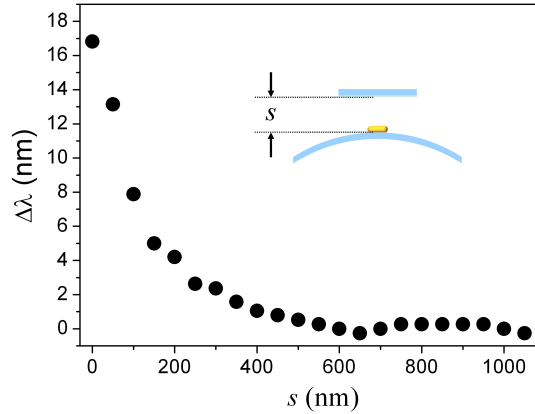


Figure 6.10: The change in the plasmon resonance wavelength ($\Delta\lambda$) as a function of the distance (s) between the two substrates.

We now discuss the curve in Fig.6.10, starting from contact and increasing the gap distance. As the air gap is increased, we find a significant blue shift of 15 nm, corresponding to a decrease of the shielding of plasmon charges by polarization charges of the upper substrate. Alternatively, this effect may be seen as an interaction between the plasmon charges and their (delayed) electrostatic image charges in the second interface. This shift reaches an almost constant value for gaps larger than 400 nm, with possibly a small oscillating contribution already observed by Hakanson et al.²⁵⁰, and related to the well-known oscillations of the radiative lifetime a few wavelengths away from a dielectric interface.^{244,253–256}

In order to check if there are any changes in the polarization anisotropy and the orientation of the particle before and after the two substrates get in mechanical contact, we performed polarization dependent measurements as we performed previously in Chapter 5. Shortly, we recorded the photoluminescence spectrum of the same single gold nanorod while rotating the analyzer and plotted the maximum intensity of the longitudinal plasmon resonance as a function of the detection polarization. This experiment yields the curves in Fig.6.9 B and a modulation depth of 0.9 confirming a dipole behavior. Fig.6.9 B also shows that there was no significant change in the anisotropy

and orientation of the nanorod.

6.4 Conclusions

We have investigated the effect of an approaching dielectric interface on the luminescence properties of individual gold nanorods. We observe a red-shift in the luminescence plasmon resonance wavelength of a gold nanorod while the distance between the two substrates is decreased. The significant changes in the plasmon resonance are observed for distances less than 400 nm. The maximum change in the plasmon resonance wavelength is about 15 nm. The observed effect is reversible. With this knowledge, gold nanorods can find applications in areas ranging from biology to tribology. For instance, single gold nanorods can be used for sensitive measurement of distances between dielectric surfaces and they can serve as asperity sensors. Molecular contacts can be monitored by following the changes in the luminescence (or scattering) spectra of individual nanorods. In this way, one can study the real contact area as a function of the distance between the two substrates.